land

MDPI

Article

Spatiotemporal Characteristics and Influencing Factors of Urban Heat Island Based on Geographically Weighted Regression Model: A Case Study of Urumqi City

Yunfei Ma [1,2], Yusuyunjiang Mamitimin [1,2,*], Bahejiayinaer Tiemuerbieke [1,2], Rebiya Yimaer [1,2], Meiling Huang [1,2], Han Chen [1,2], Tongtong Tao [1,2] and Xinyi Guo [1]

[1] College of Geography and Remote Sensing Sciences, Xinjiang University, Urumqi 830017, China; grmayunfei@163.com (Y.M.); jayana1020@xju.edu.cn (B.T.); rby0217@163.com (R.Y.); hhmmll213@163.com (M.H.); 15228155453@163.com (H.C.); qlvariy1229@163.com (T.T.); 15292633585@163.com (X.G.)

[2] Key Laboratory of Smart City and Environment Modeling of Higher Education Institute, Urumqi 830017, China

* Correspondence: y_mamitmin@163.com; Tel.: +86-15276862217

Abstract: Rapid urbanization threatens the ecological environment and quality of life by significantly altering land use and land cover (LULC) and heat distribution. One of the most significant environmental consequences of urbanization is the urban heat island effect (UHI). This study investigated the spatiotemporal characteristics of the SUHI and its relationship with land use types from 2000 to 2020 in Urumqi City, located in an arid and semi-arid region of northwestern China. Additionally, the ordinary least squares (OLS) and geographically weighted regression (GWR) models were used to quantify the relationship between the land surface temperature (LST) and influencing factors. The results showed that the area of the lower surface temperature classes has decreased significantly. In comparison, the area of the higher surface temperature classes has experienced a steady rise over the last two decades. From 2000 to 2020, the share of the area occupied by the temperature range <30 °C decreased by 67.09%. In addition, the LST varied significantly from one category of land use to another. The average LST of built-up land and unused land was higher than the average LST of other land use types in all years, while the average LST of grassland, forest land, and water bodies was significantly lower. Finally, the results of the GWR model showed that R^2 and adjusted R^2 of the GWR were 0.75 and 0.73, obviously larger than the 0.58 of the OLS models. The GWR model's higher R^2 and adjusted R^2 compared to the OLS model indicates that the relationship between LST and the influencing factors underlying the model may exhibit spatial non-stationarity, and the GWR model performs better than the OLS model. The results of both OLS and GWR models show that the normalized difference vegetation index (NDVI) and slope were negatively correlated with LST, while the urban index (UI) and normalized difference built-up index (NDBI) were positively correlated with LST. The findings of the study indicate that increasing green spaces and limiting the unplanned expansion of urban areas are effective measures to mitigate the UHIs in the study area. The results of the study may provide valuable insights into the spatiotemporal characteristics of the UHI and its drivers. Understanding the spatiotemporal characteristics of the UHI can help urban planners, policymakers, and scientists develop more effective urban cooling strategies and improve the urban thermal environment.

Keywords: arid and semi-arid regions; Urumqi City; land use and land cover; land surface temperature; urban heat island; geographically weighted regression

check for updates

Citation: Ma, Y.; Mamitimin, Y.; Tiemuerbieke, B.; Yimaer, R.; Huang, M.; Chen, H.; Tao, T.; Guo, X. Spatiotemporal Characteristics and Influencing Factors of Urban Heat Island Based on Geographically Weighted Regression Model: A Case Study of Urumqi City. *Land* **2023**, *12*, 2012. https://doi.org/10.3390/land12112012

Academic Editors: Dayi Lai, Bo Hong, Yongxin Xie, Kuixing Liu and Zhi Gao

Received: 30 September 2023
Revised: 29 October 2023
Accepted: 31 October 2023
Published: 2 November 2023

Copyright: © 2023 by the authors. Licensee MDPI, Basel, Switzerland. This article is an open access article distributed under the terms and conditions of the Creative Commons Attribution (CC BY) license (https://creativecommons.org/licenses/by/4.0/).

1. Introduction

With the development of modern society, a large influx of people to cities has led to increasing urbanization around the world [1,2]. On the one hand, rapid urbanization has led to significant improvements in basic infrastructure, public services and living conditions for

the population [3]. On the other hand, it has created many problems, such as environmental pollution, reduction of biological diversity, and human health problems that need to be solved [4]. The large number of building facilities in urban centers can significantly increase land surface temperature (LST), which has become a significant concern for geographers and urban planners [5]. The urban land surface consists of vegetation (grassland, forest, bush jungle, orchards, farmland), water bodies, impervious materials, soils and rocks, and the increase in urban surface temperature caused by large areas of waterproof materials in the city contributes to forming an urban heat island (UHI). The UHI affects the urban environment, air quality, and growth and development of plants and animals, and directly or indirectly affects people's health [6–8]. The climate change assessment report published by the United Nations Intergovernmental Panel on Climate Change (IPCC) states that the best estimate of global warming would reach 1.5 °C in the next twenty years, and the world will inevitably face multiple climate hazards. Thus, a better understanding of the spatiotemporal characteristics and influencing factors of UHI effects is necessary to support climate change mitigation efforts and urban planning and management [9–12].

The scholar Manley first formally defined the UHI in the 1950s [13]. The UHI is a phenomenon in which the LST of urban areas is higher than that of the surrounding non-urban environment due to urbanization [14]. The energy basis for the formation of UHIs is the heat balance, which is influenced by a combination of natural and anthropogenic factors, emphasizing land use and land cover (LULC) changes [15,16]. Urban expansion causes dramatic changes in the urban land surface in the urbanization process, and the original rural land undergoes irreversible transformation and gradually becomes urban land. This process replaces natural soil and vegetation with impermeable cement, asphalt, brick, tile, etc. [17,18]. This change leads to a drastic change like thermal radiation in the urban substrate, which results in a significant difference in solar radiation between urban and suburban areas. Thus, there is a corresponding quantitative relationship between UHI and LULC. Scholars have recently conducted much research to quantify the relationship between UHI and LULC. Chen et al. have studied the urbanization process through changes in LST and land use using Indiana, USA, as an example [19]. Jiang and Zha have analyzed the quantitative relationship between LST and land use in urban areas of Hefei City using Landsat TM images as the data source, and the study showed that the spatial distribution of SUHIs in Hefei City was consistent with the contour of urban construction land. Liu et al. have analyzed the relationship between the SUHI effect and land use changes in 11 jurisdictions in Wuhan city by applying remote sensing and GIS techniques and found that the increase in built-up land was an important factor in the expansion of SUHI intensity [20].

Remote sensing (RS) has proven to be a powerful technology in the domain of environmental studies. It has been widely used in the study of urban climate because of its ability to generate continuous real-time data on a large scale [21,22]. RS technology offers a simple and consistent approach for researching the thermal environment of cities, as it can be used to acquire spatially continuous information over a wide region and historical data, thus overcoming the constraints of the traditional process of ground-based observation by a small number of meteorological stations [11]. At present, NOAA/AVHRR, EOS/MODIS, ASTER, and Landsat TM/ETM+ are commonly used data sources in the research on the SUHI effect. Among them, the Landsat TM/ETM+ sensors have a relatively high spatial resolution. They can accurately reflect the spatial differences in heat island intensity within cities, so they are widely used in SUHI research. Xu et al. quantitatively analyzed the temporal and spatial characteristics of the SUHI effect in Shenzhen City, China, using Landsat-7 and Landsat-8 images between 2014 and 2019 [23]. Tesfamariam et al. assessed the spatiotemporal variation in SUHI effects in Mekelle City, Northern Ethiopia, using Landsat TM, ETM+, and OLI sensor satellite images [24]. Welegedara et al. explored the spatiotemporal changes in the SUHI effects in Edmonton City, Canada, using Landsat-5 and Landsat-8 satellite images [25].

Studies on the factors influencing the UHI focus on revealing the intensity of each factor's contribution to the UHI. Many factors affect the LST, including vegetation cover, water bodies, slope, elevation, and urban construction intensity. Rizwan et al. divided the influencing factors into two major categories: controllable and uncontrollable [26]. The controllable factors include human-related anthropogenic heat, air pollution, design-related urban sky view factors, green space coverage, building materials, etc. Uncontrollable factors include anticyclone, season, wind speed, cloudiness, etc. Tang et al. have analyzed the relationship between vegetation cover, normalized difference water index (NDWI), normalized difference built-up index (NDBI), and LST in Zhengzhou, China [27]. They found that the NDBI was positively correlated with LST, while the NDWI was negatively correlated with LST. Hung et al. have studied the spatial distribution characteristics of the SUHI effect intensity in 18 major Asian cities using TERRA/MODIS data and Landsat image series and pointed out the correlation between LST and vegetation cover [28]. Shahfahad et al. conducted a study on the seasonal variation in LST in eight cities located in the semi-arid region of India. Their findings revealed that soil moisture has a greater influence on SUHI than vegetation conditions in semi-arid environments [29]. Enete et al. have studied the effect of urban tree species on SUHI effect reduction in Enugu, Nigeria, and found that urban tree species reduced the temperature between 5 and 8 °C [30]. Zhang et al. studied the cooling effects of different green spaces and found that the average cooling range of various green spaces ranged from 1.2 to 9.5 °C. They also found that green spaces' SUHI effect mitigation function was related to the type of green space, tree species, species composition, and stand density [31].

Nowadays, a variety of mathematical approaches and models are being used by researchers to examine the connection between UHI changes and influencing factors, which mainly include Pearson correlation analysis, principal component analysis (PCA), ordinary least squares (OLS) regression analysis, the geographical weighted regression (GWR) model, grey correlation analysis, and geo-detector analysis [32–34]. Among them, the GWR model proposed by Brunsdon et al. has been applied in geography and its related disciplines [35]. Wang et al. investigated the relationship between land cover and surface temperature in the Beijing-Tianjin-Tanggu urban agglomeration by establishing a GWR model, and the results showed that the land cover ratio and LST were significantly correlated [36]. Kashki et al. evaluated the relationship between LST and influencing factors in Shiraz City, Iran. They found that the GWR model had the spatial distribution of the LST compared with OLS [37]. Li et al. analyzed the correlations between SUHI and driving factors in 419 major cities worldwide [38]. They found that the GWR model had a higher coefficient of determination (R^2) than OLS and stepwise multiple linear regression (SMLR).

Although extensive research has been carried out on the spatiotemporal patterns and influencing factors of LST globally and in China, there are a lack of investigations on cities in arid and semi-arid regions of northwestern China. As the capital of Xinjiang Uygur Autonomous Region, Urumqi is a world-famous route along the ancient Silk Road and a transportation hub between Xinjiang and mainland China [39]. In the 21st century, due to the ongoing implementation of the national development strategy, the population of Urumqi has been growing [40]. As a result, there has been a growing trend of urban population, leading to a steady increase in urbanization [41]. However, this city belongs to a temperate continental arid climate with a fragile ecological environment, and the ecological problems caused by urban heat islands are prominent. Therefore, the purpose of this research was to (1) evaluate the spatial and temporal distribution of UHI intensity between 2000 and 2020 in Urumqi City in the arid and semi-arid areas of northwestern China; (2) explore the relationship between LST and land use; (3) establish a GWR model to investigate the spatial relationship between the LST and relevant driving forces, and recommend possible solutions for mitigating the UHI in the study region. This study attempts to provide insights into the spatiotemporal characteristics of the UHI in Urumqi. By doing so, it tries to provide a theoretical foundation for mitigating the impact of UHI in the city and ultimately enhance the quality of life and living conditions.

2. Materials and Methods

2.1. Study Area

Urumqi is located at 86°37′33″–88°58′24″ E, 42°45′32″–45°00′00″ N, which is the farthest from the coastline among all cities in the world. It is the capital of the Xinjiang Uyghur Autonomous Region and the core city of the urban agglomeration on the northern slope of Tianshan Mountain (Figure 1). Urumqi is in a mid-temperate continental arid climate zone, with significant variations in temperature, sharp fluctuations in cold and heat, and scant precipitation. The highest temperatures in the area occur in July and August, with an average temperature of 25.7 °C. Winters are cold and long, with average temperatures reaching −15 °C in January. With the rapid social and economic development, the urban and rural residents of Urumqi are increasing year by year, and people's living standards and quality of life are improving. The share of population and employment in the territory is rising, with the resident population exceeding 3 million, according to the sixth national census. The city's per capita GDP exceeds $4000, placing it among the top provincial capitals in western China.

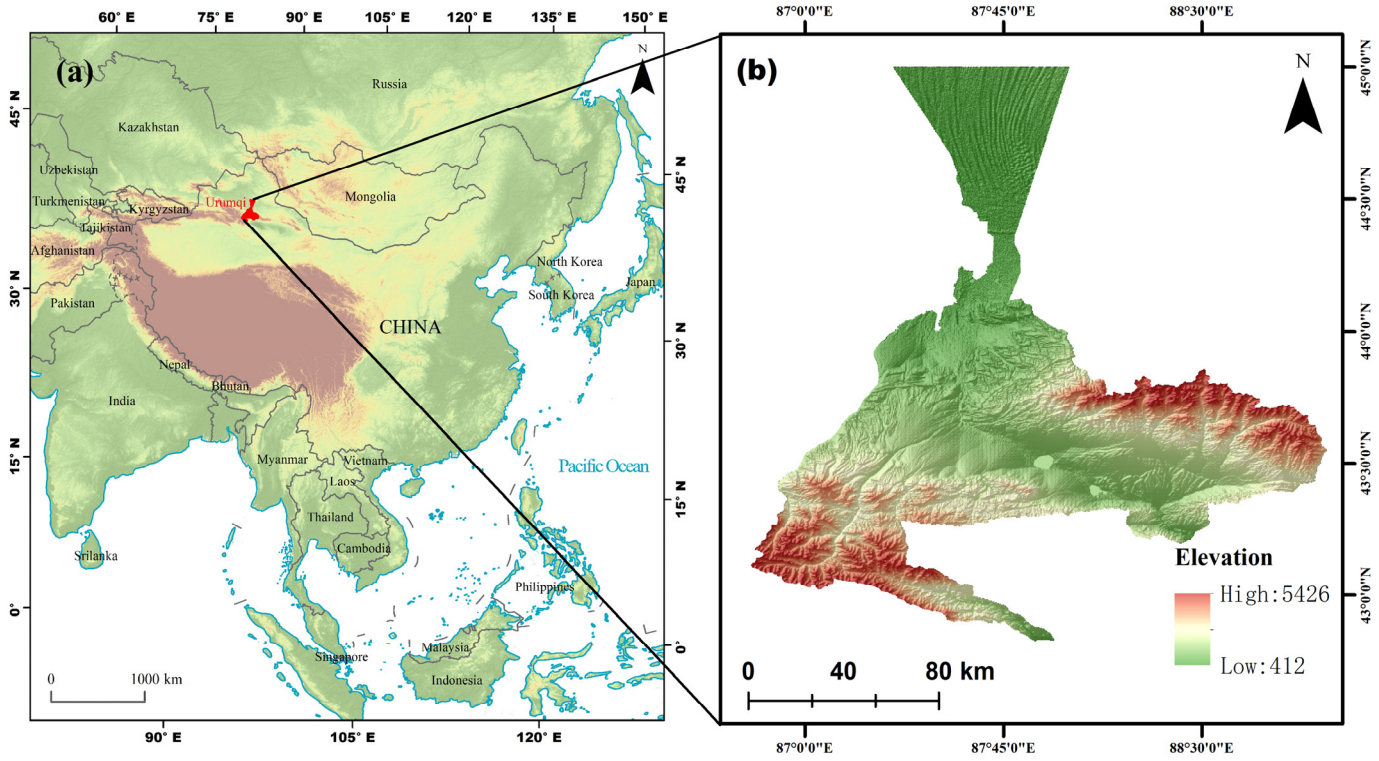


Figure 1. Geographical location (**a**) and topographic map (**b**) of the study area.

2.2. Data Sources

Landsat remote sensing data for 2000–2020, land use data for 2000–2020, digital elevation model (DEM) data at a resolution of 30 m, and the administrative boundary vector file were used in this study. Landsat remote sensing data and DEM data and the administrative boundary vector file of the study area were sourced from the Geospatial Data Cloud Platform of the Computer Network Information Center of the Chinese Academy of Sciences (https://www.gscloud.cn (accessed on 10 September 2022)). The spatial resolution of Landsat remote sensing data was 30 m, the selected data were concentrated from June to September, and the cloud cover was less than 10%, which met the requirements of the study (Table 1). The administrative boundary of the study area did not change during the study period. Therefore, the administrative boundary vector file for the year 2018 was used in this study. Land use data were obtained from the Institute of Geographical Sciences and Resources, Chinese Academy of Sciences (https://www.resdc.cn (accessed on

13 September 2022)) with a resolution of 30 m. Based on the LULC classification system of the Chinese Academy of Sciences, the land use types of Urumqi in 2000, 2010, 2015, and 2020 were classified into six categories: cropland, grassland, forest land, built-up land, water bodies, and unused land.

Table 1. Descriptions of Landsat TM/OLI images used in the study.

Years	Sensor	Path/Row	Acquisition Time	Cloud Cover
2000	Landsat-5 TM	142/029	14 June 2000 (12:26:04)	0.00
		142/030	2 September 2000 (12:28:10)	1.00
		143/029	25 September 2000 (12:34:16)	3.00
		143/030	25 September 2000 (12:34:40)	2.00
2010	Landsat-5 TM	142/029	13 August 2010 (12:40:04)	0.01
		142/030	13 August 2010 (12:40:29)	0.03
		143/029	20 August 2010 (12:46:14)	0.00
		143/030	20 August 2010 (12:46:38)	6.36
2015	Landsat-8 OLI/TIRS	142/030	12 September 2015 (12:50:03)	2.78
		143/029	3 September 2015 (12:55:44)	0.07
		143/030	3 September 2015 (12:56:16)	2.28
2020	Landsat-8 OLI/TIRS	142/029	8 August 2020 (12:49:43)	5.81
		142/030	8 August 2020 (12:50:07)	5.28
		143/029	14 July 2020 (12:55:47)	0.17
		143/030	31 August 2020 (12:56:28)	7.10

2.3. Data Processing

2.3.1. Data Pre-Processing

Radiometric calibration and atmospheric correction were performed on Landsat satellite image data during pre-processing. The Radiometric Calibration tool in the ENVI5.3 software was utilized to convert the digital numbers (*DN*) of Landsat images to corresponding thermal radiation intensity values (L_λ) [42]. The equations can be written as:

$$L_\lambda = \left(\frac{L_{max\lambda} - L_{min\lambda}}{255} DN\right) + L_{min\lambda} \quad (1)$$

where $L_{max\lambda}$ and $L_{min\lambda}$ are the minimum and maximum radiation values, respectively, which can be obtained from the metadata of Landsat images.

FLAASH Atmospheric Correction under the Atmospheric Correction Module column of Radiometric Correction in the ENVI5.3 toolbar was used to perform an atmospheric correction process for the thermal infrared band of Landsat images.

2.3.2. Retrieval of the LST

In this study, the atmospheric correction method (radiative transfer equation) was used for surface temperature inversion of Landsat images of Urumqi City. The atmospheric correction approach is a traditional algorithm derived from the atmospheric radiative transfer model. Firstly, the radiance value was converted into brightness temperature with the following equation:

$$P(T_S) = \frac{\left[L_\lambda - L_\uparrow - \tau(1-\varepsilon)L_\downarrow\right]}{\tau\varepsilon} \quad (2)$$

where $P(T_S)$ is the brightness temperature in Kelvin (K). $L_\uparrow$ is the atmospheric upwelling radiance, and $L_\downarrow$ is the atmospheric downwelling radiance. τ is the atmospheric transmission, while ε is the surface emissivity. $L_\downarrow$, $L_\uparrow$ and τ were obtained from the query website published by NASA (http://atmcorr.gsfc.nasa.gov (accessed on 20 September

2022)). Surface emissivity can be calculated by the NDVI threshold method proposed by Sobrino [43]. The mathematical expression can be written as:

$$\varepsilon = 0.004P_V + 0.986 \quad (3)$$

where ε is the surface emissivity, while P_V is the vegetation cover.

Secondly, vegetation cover was calculated based on the formula proposed by Zhang [44] with the following equation:

$$P_V = \frac{NDVI - NDVI_{Soil}}{NDVI_{Veg} - NDVI_{Soil}} \quad (4)$$

where $NDVI$ stands for the normalized difference vegetation index, $NDVI_{Soil}$ is the $NDVI$ value of bare soil, and $NDVI_{Veg}$ is the $NDVI$ of the regions with full vegetation. The values 0.05 and 0.70, respectively, were used as the values for $NDVI_{Soil}$ and $NDVI_{Veg}$ in the study.

Finally, the LST can be obtained by using the Planck function after obtaining the brightness temperature, which is calculated as:

$$LST = \frac{K_2}{ln\left[\frac{K_1}{P(T_S)+1}\right]} - 273.15 \quad (5)$$

where LST represents the land surface temperature measured in degrees Celsius, while K_1 and K_2 are constants whose values can be obtained from the MTL file.

2.3.3. Selection and Calculation of the Influencing Factors

According to the existing studies on the LST driving mechanism, four elements, including NDBI, UI, NDVI in 2020, and slope, were selected in this study (Figure 2). The selection of these drivers was based on their relevance to the research question, the availability of the data, and the principles of validity and reliability. The definitions and equations for calculating these factors are shown in Table 2.

Table 2. The definition of the selected influencing factors.

Index	Definition	Equation	
NDBI	NDBI is a remote sensing index used to measure the density of buildings on the ground surface. The higher its value, the higher the density of buildings in the corresponding area [45].	$NDBI = \frac{NIR-SWIR}{NIR+SWIR}$	(6)
UI	UI is an indicator that describes the size structure of a country or region's cities [46].	$UI = \frac{SWIR_2-NIR}{SWIR_2+NIR}$	(7)
NDVI	NDVI is the premier indicator for determining vegetation growth and cover [47].	$NDVI = \frac{\rho_{NIR}-\rho_R}{\rho_{NIR}+\rho_R}$	(8)
Slope	The slope is the measure of the inclination of the actual ground (D) when compared to the horizontal plane (H).	$S=H/D$	(9)

Figure 2 shows the spatial distribution of each driver in Urumqi. The NDVI is generally consistent with the distribution of vegetation in the study area. The slopes of Urumqi are widely distributed in the mountainous regions on the eastern, southern, and western sides of the city. It is evident that the distribution of NDBI and UI is related to the urban substrate.

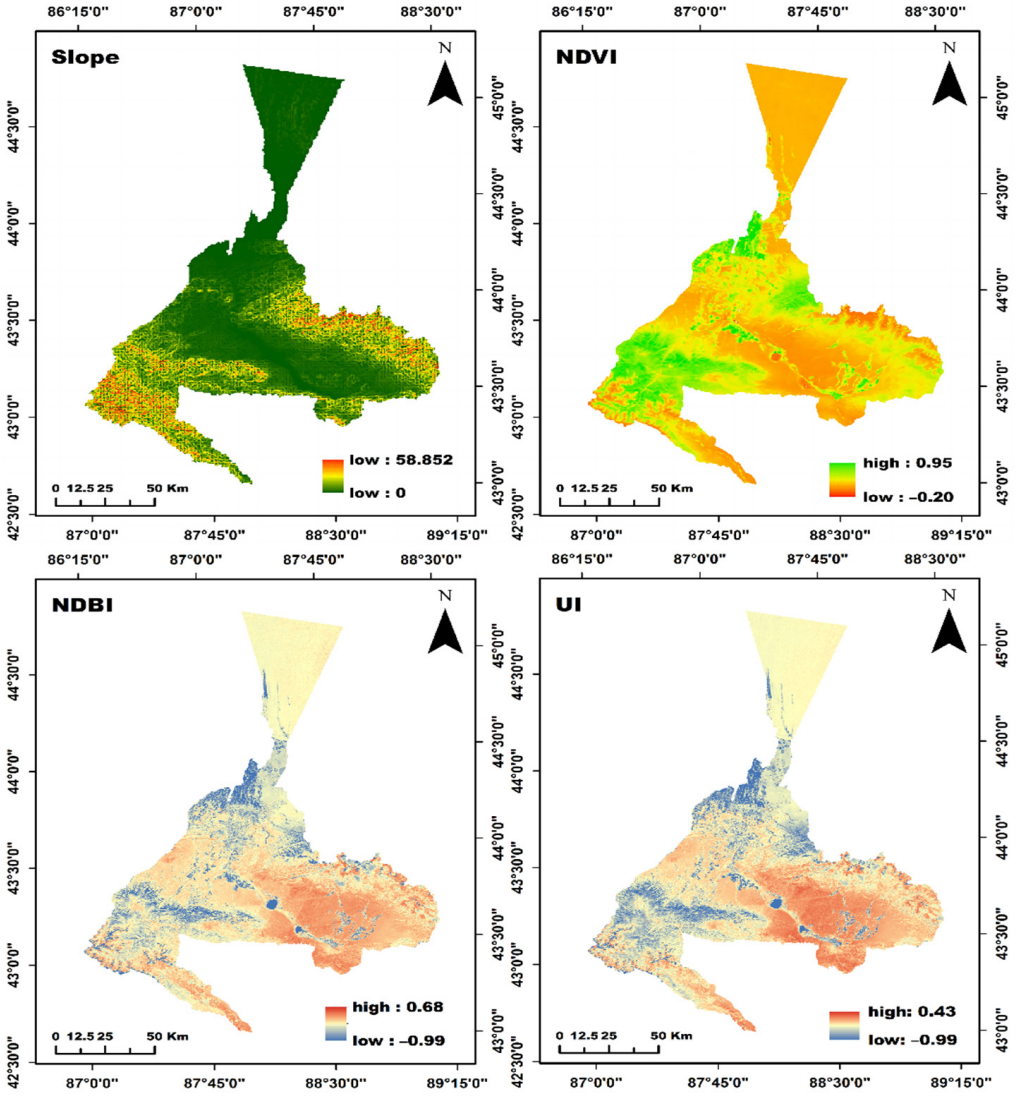


Figure 2. Spatial distribution of selected influencing factors in Urumqi.

2.3.4. OLS and GWR Model

The OLS estimation method, which has global spatial stability, is based on the assumption of a linear regression relationship, thereby generating a unique regression equation that matches all variables. The specific equation is as follows:

$$Y = \beta_0 + \beta_1 x_1 + \beta_2 x_2 + \cdots + \beta_k x_k + \varepsilon \tag{10}$$

where Y represents the dependent variable that indicates the surface temperature, while x_1–x_k are independent variables indicating the influencing factors related to the surface temperature. β is the coefficient to be estimated, responding to the linear correlation between Y and x, where β_0 denotes the intercept constant, β_1–β_k denotes the correlation coefficient between each influence factor of x_1–x_k and the surface temperature; ε is the error term that conforms to the positive terrestrial distribution. The matrix equation for the least squares estimation of the parameters is as follows:

$$\widehat{\beta} = \left(X^T X\right)^{-1} X^T Y \tag{11}$$

where X is a design matrix of the independent variables of dimension $n \times (k + 1)$, while Y is a column vector of observed dependent variables of dimension $n \times 1$. n is the number of data points, while T is a vector of $n + 1$ local regression coefficients.

When OLS is used to estimate parameters, it is assumed that the observations are independent and unaffected by other factors. When the residuals of OLS regression results are analyzed using the Morans' I index, it is necessary to use local regression methods to improve model stability and prediction accuracy if the residuals are spatially autocorrelated.

The OLS model is a global regression method that cannot account for spatial heterogeneity between the dependent and independent variables. The GWR model, on the other hand, improves the OLS model by incorporating spatial variation into the coefficient estimation process of the explanatory variables in the regression model [48]. Unlike traditional global regression models, GWR can analyze data characterized by spatially varying relationships (non-stationarity) with dependent variables [49]. GWR constructs a local model to explain the spatial relationship between the relevant dependent and predictor variables [50] with the following equation:

$$y_i = \beta_0(u_i, v_i) + \sum_{ik} \beta_k(u_i, v_i) X_{ik} + \varepsilon_i \quad (12)$$

where y_i, X_{ik} and ε_i are the dependent variable, the independent variable, and the random error at point i, respectively. The coordinates represent the position (u_i, v_i) of the fixed issue i. The coefficient $\beta_k(u_i, v_i)$ indicates the different weights at that location, and $\beta_0(u_i, v_i)$ shows the geographically diverse intercepts. Thus, the GWR technique enhances the global regression model by integrating geographic location parameters, allowing for the production of local coefficients and elucidation of spatial non-stationarity. The $\beta_0(u_i, v_i)$ and $\beta_k(u_i, v_i)$ are estimated by calculating an unbiased set of observations, wherein the weight matrix is employed to assign varying weights to the comments [51]. The distinct $\beta_k(u_i, v_i)$ values at different locations differentiate the GWR from the OLS. The distance to the fixed point i greatly impacts the weight matrix.

$$\beta_0(u_i, v_i) = \left(X^T W(u_i, v_i) X\right)^{-1} X^T W(u_i, v_i) Y \quad (13)$$

The weight matrix ($W(u_i,v_i)$) is generally generated using a Gaussian function of the following equation:

$$W(u_i, v_i) = e^{-0.5\left(\frac{d(u_i,v_i)}{b}\right)^2} \quad (14)$$

where d is the distance between observed data points, which can usually be computed using Euclidean distance or other distance metrics, and b^2 is the bandwidth parameter, which controls the rate of decay of the weights. A smaller b^2 causes the weights to decay faster, and only nearby observations have a significant effect on the model, and a larger value of b^2 causes the weights to decay more slowly, and more distant observations have some effect on the model.

The GWR model in this study was constructed using the GWR tool in ArcGIS 10.8 software, and the Akaike Information Criterion (AIC) was used to determine the most bandwidth. Compared with OLS, GWR produces more accurate estimates. Also, the model results reflect the local situation because the sample spatial units can correspond precisely to the coefficients and thus can better restore some regional characteristics of the relationship between the original independent variables [50].

2.4. SUHI Intensity Classification

The most common method for modeling the effects of urban sprawl and land use change on SUHII is to calculate the difference between urban and rural temperatures [52]. However, in the context of local zone (LCZ) concept, SUHII is defined as the surface temperature difference between built-up areas and green spaces [53]. Since the LST of greenfield sites also showed variation, the average LST of greenfield sites (i.e., cropland,

forest land, and grassland) was used as the reference temperature for SUHII mapping. Therefore, *SUHII* was calculated for each combined pixel using Equation (15) [54].

$$SUHII_i = T_{bui} - T_{gs} \quad (15)$$

where $SUHII_i$ is the *SUHII* at built-up pixel i, T_{bui} is the LST at built-up pixel i, and T_{gs} is the average LST of the greenfield pixels. The further derivation of the SUHII for the whole study area is given in the following Equation (16).

$$SUHII = \frac{1}{n}\sum_{i=1}^{n} SUHII_i \quad (16)$$

where $SUHII_i$ denotes the *SUHII* at pixel i and n denotes the total number of accumulated pixels.

In this study, SUHII strengths are categorized into five categories, i.e., no SUHII (<0.00), low SUHII (0.00–2.00), moderate SUHII (2.00–4.00), high SUHII (4.00–6.00) and very high or extreme SUHII (>6.00) [55].

3. Results

3.1. The Spatiotemporal Characteristics of the LST

The inversion results of LST in Urumqi were obtained for 2000, 2010, 2015, and 2020 with the help of ENVI5.3 software (Figure 3). Based on the results of the LST inversion, the LST of Urumqi was divided into five classes: <10 °C, 10~20 °C, 20~30 °C, 30~40 °C, >40 °C. The statistical analysis of the area and percentage of the LST classes for each year are presented in Table 3. The results showed a significant variation in the LST in Urumqi, with a considerable inter-annual variation. From 2000 to 2020, the share of the area occupied by the temperature range <10 °C decreased by 9.51%, while the percentage of the space occupied by the temperature range 10–20 °C and 20–30 °C kept reducing by 25.46% and 32.12%, respectively. On the contrary, the share of the area occupied by the temperature range 30–40 °C increased by 17.48%, while the percentage of the space occupied by the temperature range >40 °C increased by 49.60%. The results indicate that the area of the lower surface temperature classes has decreased significantly. In comparison, the area of higher surface temperature classes has experienced a steady increase over the last two decades.

3.2. Analysis of Spatial and Temporal Variation in SUHII

Figure 4 and Table 4 show the spatial distribution and temporal variations of the SUHII with five temperature classes. The results showed that the SUHII is higher in the core area of Urumqi compared to the suburbs, indicating that the area has low vegetation cover and dense urban buildup. The SUHII continued to increase between 2000 and 2020. Between 2000 and 2010, the SUHII was low in all areas of Urumqi, and the proportion of areas with no SUHII, low SUHII, and moderate SUHII increased by 0.07%, 0.37%, and 0.15%, respectively. At the same time, the proportion of areas with high SUHII and areas with very high SUHII decreased by 0.17% and 0.11%, respectively. From 2010 to 2015, the SUHII increased significantly, and it can be seen that the area of very high SUHII increased significantly, mainly in the north, east and west of the built-up area, and the proportion of the increase was 3.04%, the area of high SUHII in the southern part of the built-up area increased significantly, with an overall increase proportion of 0.42%, and the proportion of the area accounted for by no SUHII, low SUHII and moderate SUHII decreased sharply, with decreasing proportions of 1.16%, 0.73% and 0.38%, respectively. From 2015 to 2020, the SUHII still remained high, and there were minor fluctuations in the SUHII for each class.

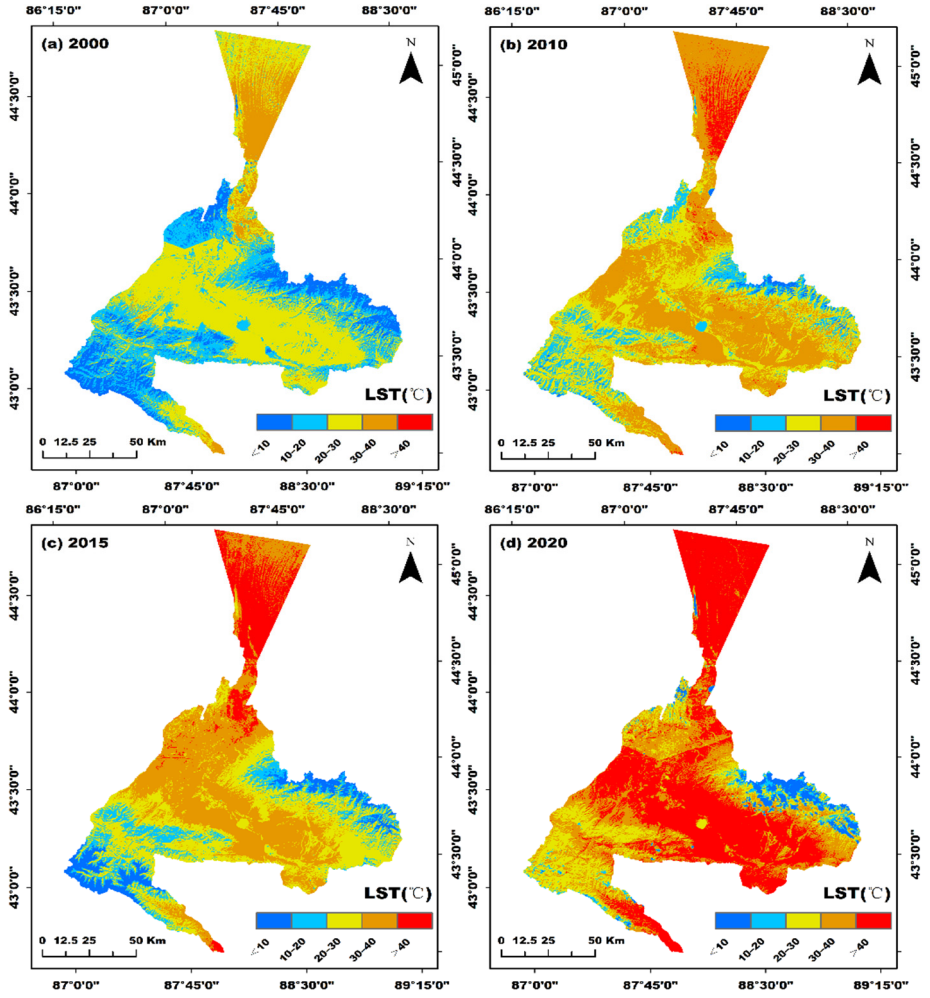


Figure 3. Spatial distribution maps of LST for Urumqi City for four consecutive years ((**a**–**d**) refers to the spatial distribution of LSTs in 2000, 2010, 2015 and 2020, respectively).

Table 3. The area and percentage of the LST classes for Urumqi City for four consecutive years.

Temperature Interval	2000		2010		2015		2020	
	Area (km^2)	Percentage (%)	Area (km^2)	Percentage (%)	Area (km^2)	Percentage (%)	Area (km^2)	Percentage (%)
<10 °C	1869.53	13.15	183.60	1.29	853.97	6.02	516.55	3.64
10~20 °C	4019.82	28.31	1510.06	10.62	1572.28	10.93	405.96	2.85
20~30 °C	6865.68	48.37	5011.69	35.30	4632.84	32.78	2308.09	16.25
30~40 °C	1447.43	10.17	6879.83	48.47	5441.92	38.32	3926.21	27.65
>40 °C	2.24	0.10	617.57	4.32	1701.97	11.96	7045.91	49.61

Table 4. Spatiotemporal variation in the areal coverage of SUHII zones.

SUHII Zones/Year	Area in Percent			
	2000	2010	2015	2020
No Data	95.92	95.61	94.22	93.77
None/No SUHII	1.27	1.34	0.18	0.44
Low	0.66	1.03	0.30	0.42
Moderate	0.88	1.03	0.65	0.84
High	0.85	0.68	1.10	1.07
Very High	0.42	0.31	3.55	3.46

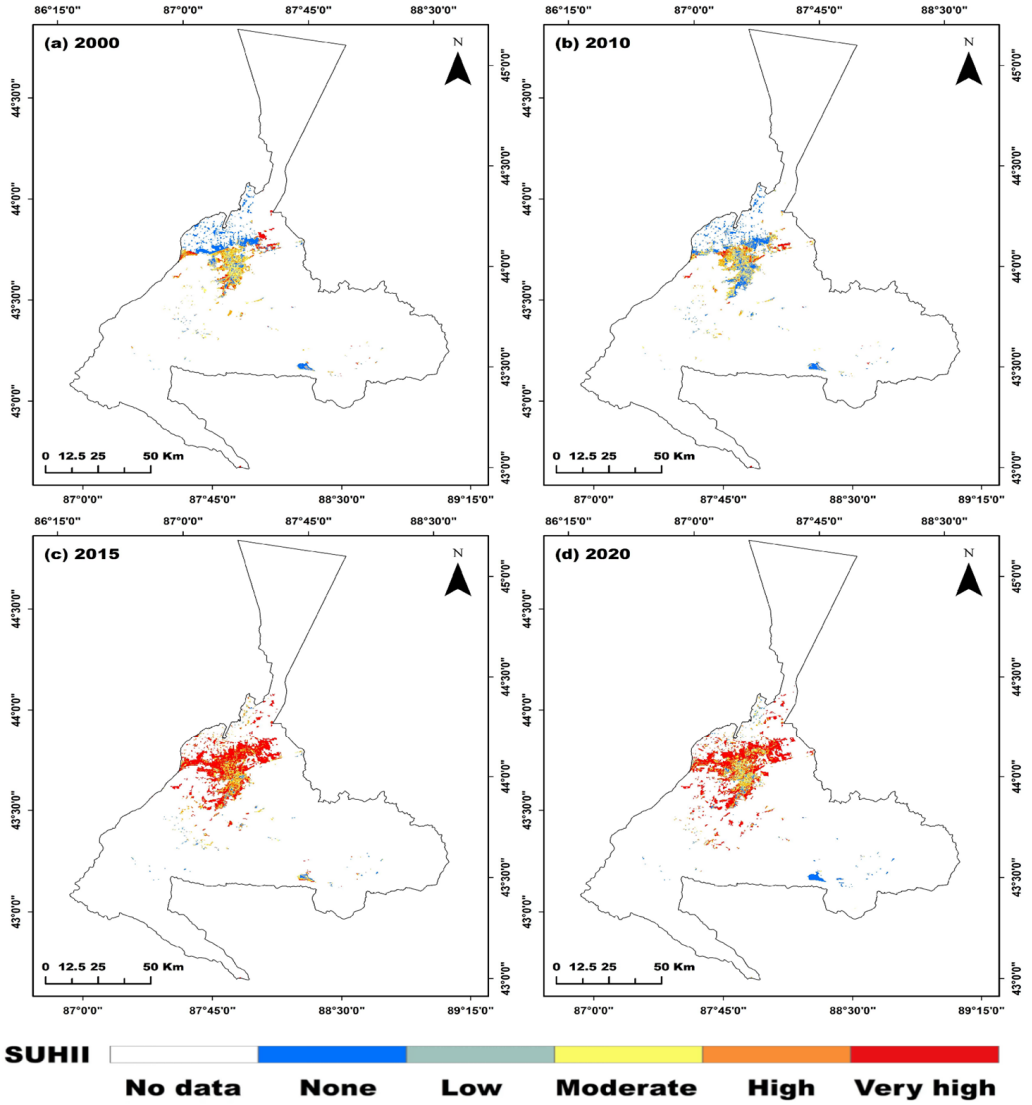


Figure 4. Spatiotemporal dynamics of SUHII (in °C) in Urumqi during 2000–2020 ((**a**–**d**) refers to the spatial distribution of SUHIIs in 2000, 2010, 2015 and 2020, respectively).

3.3. The Relationship between LULC and LST

Figure 5 and Table 5 show the spatial distribution of different LULC classes in Urumqi City and the corresponding area statistics between 2000 and 2020. Spatially, as shown in the figure, the built-up land was mainly distributed in the west and a small part in the southeast of Urumqi City. There has been a clear trend over the last 20 years for built-up land to expand to the north of the city. The cultivated land area showed a distribution pattern around the built-up land, while grassland was widely distributed in most of the study area. There were many small and dispersed water bodies throughout the study area. The unused land was mainly concentrated in the northern region and the mountainous areas of the study area's northeast, southeast, and southernmost parts. Temporally, grassland was the dominant land use type, with a share of 53.42%, 53.10%, 52.55 and 52.20% in 2000, 2010, 2015 and 2020, respectively. There was a decrease of 1.22% in the area of grasslands in 2020 compared with the year 2000. The unused land was the second most dominant land use type in the study area, with its size decreasing by 0.12% over the past 20 years. The percentage of cropland also showed a downward trend, reducing by 0.69%. The percentage of water bodies was the smallest of all land-use types, and its variation was essentially stable. The built-up land area of all land use types increased by 2.11%.

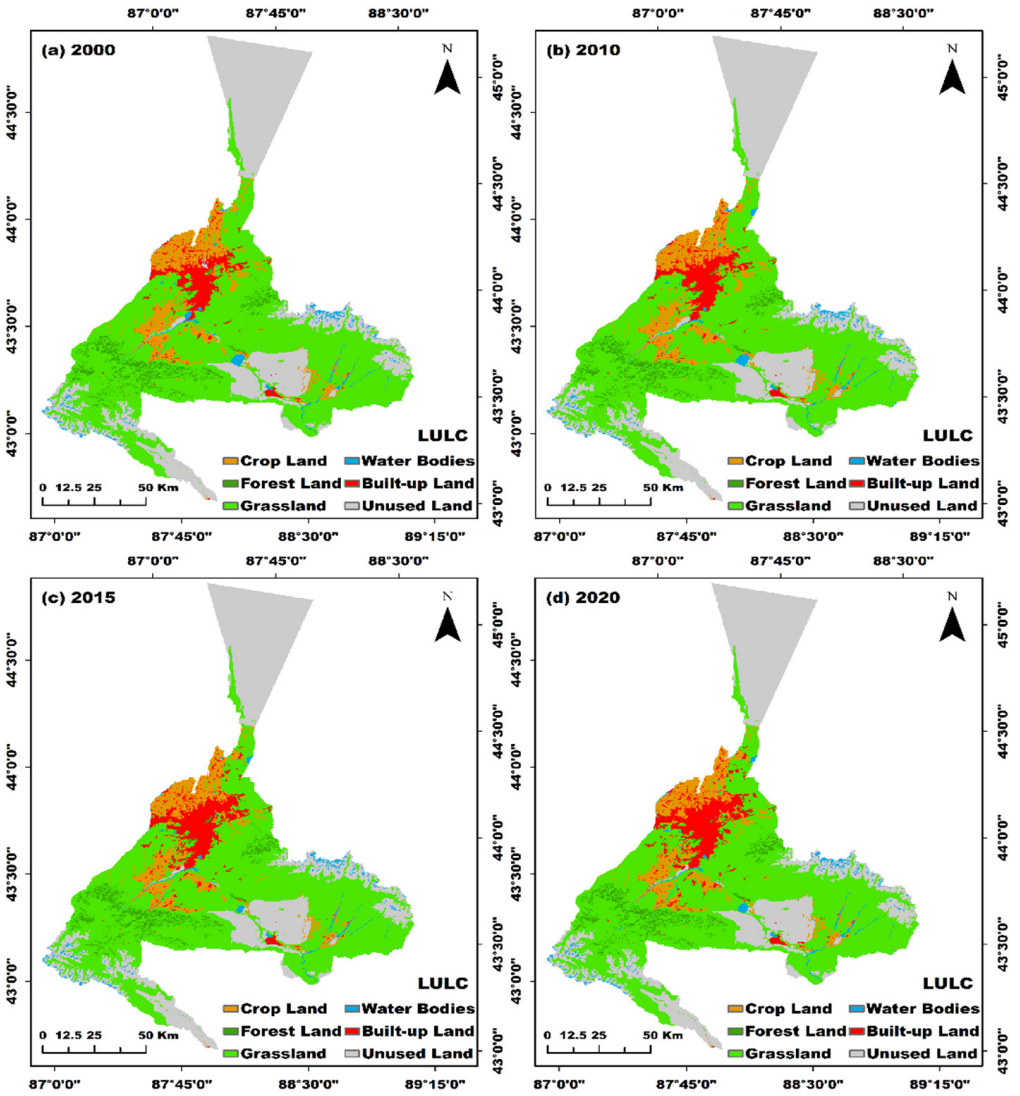


Figure 5. Spatial distribution maps of LULC for Urumqi City for four consecutive years ((**a**–**d**) refers to the spatial distribution of land use in 2000, 2010, 2015 and 2020, respectively).

Table 5. Proportion of land use area in Urumqi by year.

Land Use Type	2000		2010		2015		2020	
	Area (km^2)	Percentage (%)	Area (km^2)	Percentage (%)	Area (km^2)	Percentage (%)	Area (km^2)	Percentage (%)
Cropland	1221.01	8.60	1234.96	8.70	1157.49	8.13	1123.45	7.91
Forest Land	403.89	2.84	410.30	2.89	408.15	2.87	408.38	2.88
Grassland	7587.70	53.42	7541.62	53.10	7481.97	52.55	7413.27	52.20
Water Bodies	234.98	1.65	229.85	1.65	209.34	1.47	220.78	1.55
Built-up Land	584.66	4.12	626.45	4.41	822.15	5.77	884.59	6.23
Unused Land	4170.49	29.36	4159.55	29.29	4158.54	29.21	4152.26	29.24

The SUHI is closely related to the land cover type and is important in studying the heat island effect. The statistical results for LST between different land use types were obtained by overlaying the land use data and LST of Urumqi City in 2000, 2010, 2015 and 2020, respectively (Figure 6). The results showed that the LST varied significantly from one category of land use to another. First, the average LST of all land uses in Urumqi increased in all years of the study period, with different rates of increase as follows: unused land >

cropland > grassland > built-up land > forest land > water bodies. Secondly, the average LST of built-up and unused land was higher than the average LST of other land use types. The average LST of grassland, forest land, and water bodies was significantly lower. Finally, the standard deviation of the LST of water bodies and unused land was more extensive each year, indicating that the LST of these two land use types varied widely and irregularly within the study area. This is mainly because the water bodies in the area studied are minor and include ice and snow, as well as the fact that there is a large area of desert and Gobi in the northern part of the study area, which leads to a significant difference in their LST. Moreover, the standard deviation of the LST was more minor for built-up land and forest land, and they had stable high- and low-temperature environments, respectively.

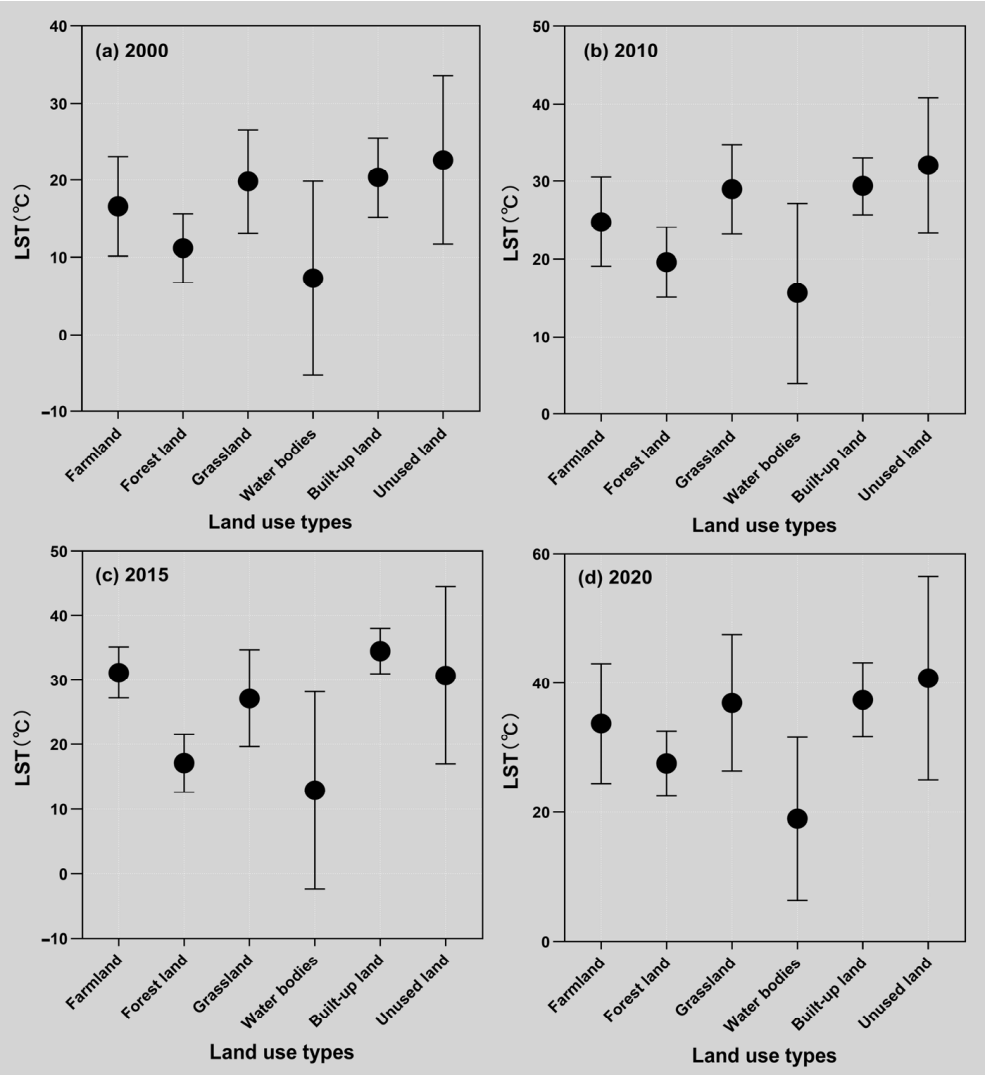


Figure 6. Differences in LSTs between land use types ((**a**–**d**) refers to the, mean LSTs and standard deviations of the different land use types in 2000, 2010, 2015 and 2020, respectively).

3.4. Results of the OLS and GWR Model

To further explore the relationship between the LST and the influencing factors, the OLS and GWR models were used in this paper, and their results were compared. The results of the OLS model are presented in Table 6. To avoid the problem of multicollinearity, the variance inflation factor (VIF) was calculated. The variance was removed if the VIF value was greater than 10. In the models used in this paper, the VIF values of the respective variables did not exceed a discount of 10. The regression model's coefficient of determination (R^2) was estimated at 0.58, indicating a good fit. For the Koenker (BP) statistic, Prob

(probability) was less than 0.01, which was statistically significant. The high value of the joint Chi-square statistic from the reported data, with a likelihood of much less than 0.01, indicated that the regression model setup was statistically significant. The above analysis shows that this regression model is statistically significant, and the fit is fair, but it is a non-stationary regression model. Meanwhile, among the explanatory variables, the NDVI and slope were negatively correlated with surface temperature, and UI and NDBI were positively correlated with surface temperature.

Table 6. The OLS model results for LST in Urumqi City.

Variables	β	SE	t	SD	R^2	Adjusted R^2	AICc
NDVI	−4.90 ***	0.16	−30.20	0.14			
NDBI	21.91 ***	0.13	164.73	0.10			
UI	7.65 ***	0.08	90.48	0.08	0.58	0.58	887,149.50
Slope	−0.11 ***	0.01	−60.71	0.01			
Intercept	53.02 ***	0.04	1065.32	0.03			

Note: β: The coefficients and intercepts, ***: $p < 0.001$ level significant.

Table 7 presents the results of the GWR model. The results show that R^2 and adjusted R2 of the GWR were 0.75 and 0.73, obviously larger than the 0.58 of the OLS model described above. The GWR model's higher R^2 and adjusted R^2 compared to the OLS model indicates that the relationship between LST and the influencing factors underlying the model may exhibit spatial non-stationarity, and the GWR model performed better than the OLS model. The results indicate that the GWR model can effectively explain the geographically heterogeneous and nonlinear relationships between LST and influencing factors.

Table 7. The GWR model results for LST in Urumqi City.

Diagnostics	Values
Residual sum of squares	2,641,758.84
AICc	872,474.52
R^2	0.75
Adjusted R^2	0.73
Bandwidth of GWR	19,569.60
Sigma	6.02

The spatial distribution of the coefficient estimates of the influencing factors in the GWR model is shown in Figure 7. Positive values in the figure indicate positive correlations, and negative values indicate negative correlations. The higher the saturation, the higher the absolute regression coefficient. As seen in Figure 7, from a quantitative point of view, the estimates of the GWR coefficients showed a spatially varying pattern. Figure 7a,b show that the slope and the NDVI negatively correlated with the LST in most areas, especially in the northern and eastern regions. Figure 7c,d show that NDBI and UI positively correlated with LST in most areas. The absolute value of the NDBI coefficient was the largest, and its contribution to increased LST was the most pronounced.

Both OLS and GWR indicated that land use type influenced the change in surface temperature during the study period. Based on the coefficient values and t-statistics, GWR further revealed the solid spatial heterogeneity of their relationships. In addition, the coefficients t of NDBI and UI in Urumqi showed that most areas had a significant relationship between surface temperature and built-up area. Overall, the regression analysis showed that the land use composition and topographic morphology of the study area were closely related to the SUHI, and the study confirmed that the increase in built-up area tended to exacerbate the SUHI. In contrast, the increase in vegetation cover intensity mitigated the SUHI. In addition, the surface temperature tended to decrease as the slope increased, since construction activities were not advisable at higher slopes.

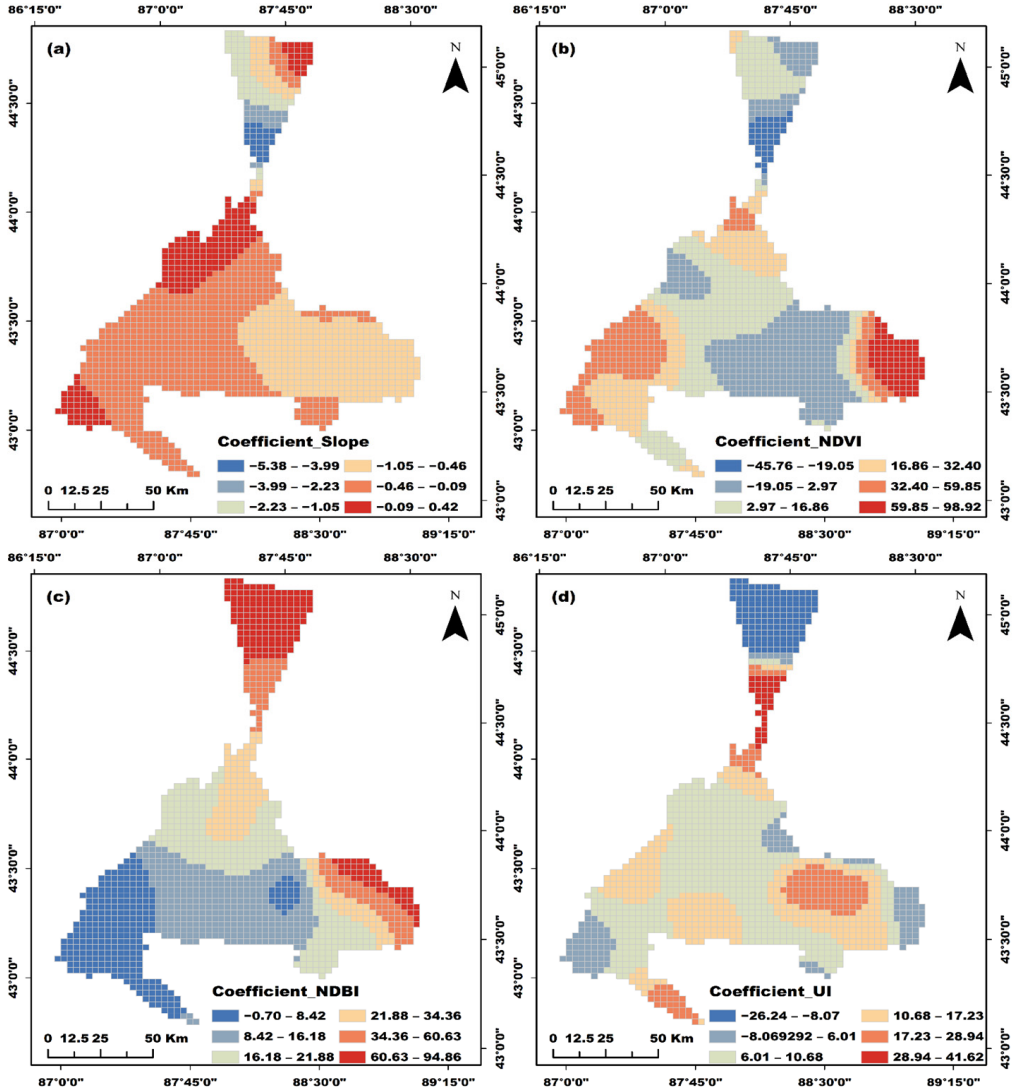


Figure 7. GWR coefficient estimates of slope (**a**), NDVI (**b**), NDBI (**c**), UI (**d**).

4. Discussion

4.1. Analysis of the Relationship between LULC and LST

Urbanization leads to changes in land use and the dynamic characteristics of the urban atmosphere, which affects the formation of the UHI [33]. The study results show that the average LST of built-up land and unused land was higher than the average LST of other land use types in all years. The average LST of grassland, forest land, and water bodies was significantly lower. The difference in average LST between unused land and greenspace (cropland, forest land, and grassland) was 6.21 °C, while the difference in average LST between built-up land and greenspace (cropland, forest land, and grassland) was 6.03 °C. The results indicate that grassland, forest land, and water bodies can effectively mitigate the SUHI. In contrast, the subsurface of built-up land is very complex, and many artificial structures consisting of concrete and asphalt roads alter the thermal properties of the subsurface due to their rapid heat absorption and low heat capacity. As a result, the subsurface of built-up land warms faster than the natural subsurface consisting of greenbelt and water under the same solar radiation conditions. In addition, surface temperatures are high in all parts of the built-up land due to the dense, tall, poorly ventilated artificial structures. Unused land has a high surface temperature because it has large bare areas that absorb heat quickly [27]. Previous studies have also confirmed that the LST of built-up and unused land is higher than that of other land use types [56–58]. Ma and Peng

studied the relationship between LULC and SUHI in Kunming City, China, and found that unused land had a higher average LST than all other land use types, with a difference in mean LST of 2.45 °C between unused land and green space [59]. Cai et al. found in the study of Fuzhou City that built-up land had the highest LST, followed by unused land from 1989 to 2009, with a difference in mean LST of 1.7 °C between built-up land and green space [60]. Saha et al. mainly analyzed the spatial relationship between LULC and LST in three urban agglomerations in the eastern part of India, and found that built-up areas exhibited comparatively higher LST and SUHI, with a difference in mean LST of 4.7 °C between built-up land and green space [61]. Njoku and Tenenbaum studied the relationship between LULC and LST in Ilorin, Nigeria, and found that LST values exhibited considerable spatial and temporal variation, with the high temperature clusters evident in the built-up areas, with a difference in mean LST of 4.4 °C between built-up land and green space [62]. Moisa and Gemeda assessed the urban thermal field variance of Addis Ababa metropolitan city, Ethiopia, and found that the highest LST was recorded in low-vegetation areas, particularly on built-up areas, cropland, and bare land [63]. At the same time, Song et al. found a 3.4 °C difference between the average LSTs for built-up land and other land use types, including cropland, grassland, and forestland, using Landsat ETM+ and Quick Bird data in a SUHI study in Beijing, China [58]. The SUHI study conducted by Weng et al. in Indianapolis, USA, using Landsat ETM+ data, found that the difference in average LST between built-up land and green spaces was even higher, as much as 5.4 °C [64].

4.2. The Model Performance and Influencing Factors of SUHI

In this study, we adopted the OLS and GWR models to quantify the relationship between the SUHI and the relevant driving factors. The results show that the GWR model performed better than the OLS model, and the relationship between the LST and the influencing factors exhibited spatial non-stationarity. The findings are in line with those of other studies. For example, Li et al. investigated the relationship between surface urban heat islands and the driving factors in 419 major cities. They found that the GWR model had higher R^2 than the OLS and stepwise multiple linear regression (SMLR) models [38]. Similarly, Gao et al. explored the relationship between the SUHI effect and morphological variables. They found that the GWR model significantly improved modeling fit by capturing spatial heterogeneity compared to the OLS model [65]. In addition, the results of both OLS and GWR models show that the NDVI and slope were negatively correlated with the LST, while the UI and NDBI were positively correlated with the LST. The results of the study are consistent with other studies. A study by Ma and Peng found that the LST was negatively correlated with the NDVI and positively correlated with the NDBI in the study of the SUHI in Kunming, China [59]. Anniballe et al. studied the spatiotemporal trends of the SUHI over the city of Milan and found that SUHI was highly correlated with NDVI [66]. Derdouri et al. studied the thermal variations in eight key Moroccan cities and found that the LST was positively correlated with the NDBI and negatively correlated with the NDVI [67]. Similarly, Shahfahad et al. modeled the relationship between UHI and land use indices in Delhi and Mumbai, India. They found that the LST was negatively correlated with the NDVI and positively correlated with the NDBI [68].

4.3. Limitations and Future Work

This study investigated the spatiotemporal characteristics of the SUHI and its relationship with land use types from 2000 to 2020 in Urumqi City, in the arid and semi-arid region of northwestern China. Additionally, the OLS and GWR models were used to quantify the relationship between the LST and influencing factors. The study results can provide urban planners and policymakers with a better understanding of the spatiotemporal characteristics of the SUHI and its drivers. However, there are still limitations. First, we could not consider the SUHI's seasonal and daily characteristics due to limited access to the data source and the cloud cover. Future research may focus on the SUHI's seasonal and diurnal daily characteristics through integrating multisource data such as Landsat and

Modis. In addition, the city is a complex, dynamic system of social connections, human activities, and infrastructure. UHIs are caused by several factors, including local climate, socioeconomic conditions, urban size, and urban form [19]. However, we only considered four influencing factors in this study. Systematic research is needed to determine how these factors contribute to the formation of the UHI. Furthermore, the Landsat TM and Landsat OLI images from different Landsat sensors were used as the main data sources in this study. Remote sensing images from different Landsat sensors have different thermal infrared bands, which have some influence on the accuracy of the surface temperature inversion [69]. Therefore, further research is needed to eliminate related uncertainties, especially when precise LST change detection or temporal trends are required. Finally, the LSTs for the year 2005 were not analyzed in this study because the corresponding land use data from the Chinese Academy of Sciences were not available. This may have some impact on the consistency of temporal trends in LST in the study area.

5. Conclusions

In this study, the spatiotemporal characteristics of UHI intensity were quantified from 2000 to 2020 using Landsat remote sensing data in Urumqi City, located in the arid and semi-arid region of northwestern China. A GWR model was developed to assess the relationship between the UHI and various influencing factors. It was further compared with the OLS model. The results show that the area of the lower surface temperature classes has decreased significantly. In comparison, the area of higher surface temperature classes has experienced a steady rise over the last two decades. In addition, the LST varies considerably from one category of land use to another. The average LST of built-up land and unused land was higher than the average LST of other land use types in all years, while the average LST of grassland, forest land, and water bodies was significantly lower. Finally, the results of the GWR model show that R^2 and adjusted R^2 of the GWR were 0.75 and 0.73, obviously larger than the 0.58 of the OLS model. The GWR model's higher R^2 and adjusted R^2 compared to the OLS model indicated that the relationship between LST and the influencing factors underlying the model may exhibit spatial non-stationarity, and the GWR model performed better than the OLS model. The results of both OLS and GWR models show that the NDVI and slope were negatively correlated with LST, while the UI and NDBI were positively correlated with LST. The results of the study revealed that the increase in the LST was closely related to urban expansion, and the urban heat island effect can be significantly mitigated with the aid of green spaces. The results of the study suggest that increasing the green spaces (grassland, forest, jungle, orchards, etc.) in the city and limiting the disorderly expansion of urban areas are effective means to alleviate the UHI effect in the study area.

Author Contributions: Data curation, Y.M. (Yunfei Ma); Formal analysis, Y.M. (Yunfei Ma) and Y.M. (Yusuyunjiang Mamitimin); Funding acquisition, B.T.; Investigation, Y.M. (Yunfei Ma) and Y.M. (Yusuyunjiang Mamitimin); Methodology, Y.M. (Yunfei Ma) and Y.M. (Yusuyunjiang Mamitimin); Resources, Y.M. (Yunfei Ma); Software, Y.M. (Yunfei Ma); Supervision, Y.M. (Yusuyunjiang Mamitimin), B.T., R.Y., M.H., H.C., T.T. and X.G.; Validation, Y.M. (Yunfei Ma); Visualization, Y.M. (Yunfei Ma); Writing—original draft, Y.M. (Yunfei Ma) and Y.M. (Yusuyunjiang Mamitimin); Writing—review and editing, Y.M. (Yunfei Ma), Y.M. (Yusuyunjiang Mamitimin), B.T., R.Y., M.H., H.C., T.T. and X.G. All authors have read and agreed to the published version of the manuscript.

Funding: This research was funded by the Natural Sciences Foundation of Xinjiang Uygur Autonomous Region (Grant No. 2021D01C056) and the Xinjiang University Innovation Training Programme for Undergraduates (Grant No. XJU-SRT-22004).

Institutional Review Board Statement: Not applicable.

Informed Consent Statement: Not applicable.

Data Availability Statement: Not applicable.

Acknowledgments: We would like to thank the Natural Sciences Foundation of Xinjiang Uygur Autonomous Region and the Xinjiang University Innovation Training Programme for Undergraduates for funding this research. We also would like to thank the anonymous reviewers for their constructive comments to improve the quality of this manuscript.

Conflicts of Interest: The authors declare no conflict of interest.

References

1. Chen, M.; Lu, D.; Zha, L. The comprehensive evaluation of China's urbanization and effects on resources and environment. *J. Geogr. Sci.* **2010**, *20*, 17–30. [CrossRef]
2. Du, H.; Duoduo, W.; Wang, Y.; Zhao, X.; Qin, F.; Jiang, H.; Cai, Y. Influences of land cover types, meteorological conditions, anthropogenic heat and urban area on surface urban heat island in the Yangtze River Delta Urban Agglomeration. *Sci. Total Environ.* **2016**, *571*, 461–470. [CrossRef] [PubMed]
3. He, W.; Li, X.; Yang, J.; Ni, H.; Sang, X. How land use functions evolve in the process of rapid urbanization: Evidence from Jiangsu Province, China. *J. Clean. Prod.* **2022**, *380*, 134877. [CrossRef]
4. Uttara, S.; Bhuvandas, N.; Aggarwal, V. Impacts of urbanisation on environment. *Int. J. Res. Eng. Appl. Sci.* **2012**, *2*, 1637–1645.
5. Gaffin, S.R.; Rosenzweig, C.; Khanbilvardi, R.; Parshall, L.; Mahani, S.; Glickman, H.; Goldberg, R.; Blake, R.; Slosberg, R.B.; Hillel, D. Variations in New York city's urban heat island strength over time and space. *Theor. Appl. Climatol.* **2008**, *94*, 1–11. [CrossRef]
6. Gunawardhana, L.N.; Kazama, S.; Kawagoe, S. Impact of Urbanization and Climate Change on Aquifer Thermal Regimes. *Water Resour. Manag.* **2011**, *25*, 3247–3276. [CrossRef]
7. Liu, Y.; Yan, B.; Zhou, Y. Urbanization, economic growth, and carbon dioxide emissions in China: A panel cointegration and causality analysis. *J. Geogr. Sci.* **2016**, *26*, 131–152. [CrossRef]
8. Jain, S.; Sannigrahi, S.; Sen, S.; Bhatt, S.; Chakraborti, S.; Rahmat, S. Urban heat island intensity and its mitigation strategies in the fast-growing urban area. *J. Urban Manag.* **2020**, *9*, 54–66. [CrossRef]
9. Liu, K.; Li, X.; Wang, S.; Li, Y. Investigating the impacts of driving factors on urban heat islands in southern China from 2003 to 2015. *J. Clean. Prod.* **2020**, *254*, 120141. [CrossRef]
10. Shi, Y.; Xiang, Y.; Zhang, Y. Urban Design Factors Influencing Surface Urban Heat Island in the High-Density City of Guangzhou Based on the Local Climate Zone. *Sensors* **2019**, *19*, 3459. [CrossRef]
11. Sismanidis, P.; Bechtel, B.; Perry, M.; Ghent, D. The Seasonality of Surface Urban Heat Islands across Climates. *Remote Sens.* **2022**, *14*, 2318. [CrossRef]
12. Wang, Y.; Yi, G.; Zhou, X.; Zhang, T.; Bie, X.; Li, J.; Ji, B. Spatial distribution and influencing factors on urban land surface temperature of twelve megacities in China from 2000 to 2017. *Ecol. Indic.* **2021**, *125*, 107533. [CrossRef]
13. Manley, G. On the frequency of snowfall in metropolitan England. *Q. J. R. Meteorol. Soc.* **1958**, *84*, 70–72. [CrossRef]
14. Yang, Y.; Guangrong, S.; Chen, Z.; Hao, S.; Zhouyiling, Z.; Shan, Y. Quantitative analysis and prediction of urban heat island intensity on urban-rural gradient: A case study of Shanghai. *Sci. Total Environ.* **2022**, *829*, 154264. [CrossRef] [PubMed]
15. Li, F.-J.; Ma, A.-Q.; Ding, Y.-D.; Yang, J.-J.; Jiao, J.-C.; Liu, L.-J. Research on Urban Heat Island Effect Based on Landsat Data. *Remote Sens. Technol. Appl.* **2009**, *24*, 553–558. (In Chinese) [CrossRef]
16. Liu, W.; Yang, P.; You, H.; Zhang, B. Heat Island Effect and Diurnal Temperature Range in Beijing Area. *Clim. Environ. Res.* **2013**, *18*, 171–177. (In Chinese) [CrossRef]
17. Chen, Y.-C.; Chen, C.-Y.; Matzarakis, A.; Liu, J.-K.; Lin, T.-P. Modeling of mean radiant temperature based on comparison of airborne remote sensing data with surface measured data. *Atmos. Res.* **2016**, *174–175*, 151–159. [CrossRef]
18. Abulibdeh, A. Analysis of urban heat island characteristics and mitigation strategies for eight arid and semi-arid gulf region cities. *Environ. Earth Sci.* **2021**, *80*, 259. [CrossRef]
19. Chen, Y.; Weng, Q.H.; Tang, L.L.; Wang, L.; Xing, H.F.; Liu, Q.H. Developing an intelligent cloud attention network to support global urban green spaces mapping. *ISPRS J. Photogramm. Remote Sens.* **2023**, *198*, 197–209. [CrossRef]
20. Liu, H.; Shen, G.; Huang, Q. Evolution of urban heat island effect and its relationship with land use change in wuhan city in recent 10 years. *Resour. Environ. Yangtze Basin* **2017**, *26*, 1466–1475. (In Chinese) [CrossRef]
21. Sekertekin, A.; Bonafoni, S. Land Surface Temperature Retrieval from Landsat 5, 7, and 8 over Rural Areas: Assessment of Different Retrieval Algorithms and Emissivity Models and Toolbox Implementation. *Remote Sens.* **2020**, *12*, 294. [CrossRef]
22. Silva, J.S.; da Silva, R.M.; Santos, C.A.G. Spatiotemporal impact of land use/land cover changes on urban heat islands: A case study of Paco do Lumiar, Brazil. *Build. Environ.* **2018**, *136*, 279–292. [CrossRef]
23. Xu, X.; Pei, H.Y.; Wang, C.; Xu, Q.Y.; Xie, H.; Jin, Y.M.; Feng, Y.J.; Tong, X.H.; Xiao, C.J. Long-term analysis of the urban heat island effect using multisource Landsat images considering inter-class differences in land surface temperature products. *Sci. Total Environ.* **2023**, *858*, 159777. [CrossRef] [PubMed]
24. Tesfamariam, S.; Govindu, V.; Uncha, A. Spatio-temporal analysis of urban heat island (UHI) and its effect on urban ecology: The case of Mekelle city, Northern Ethiopia. *Heliyon* **2023**, *9*, e13098. [CrossRef]
25. Welegedara, N.P.Y.; Agrawal, S.K.; Lotfi, G. Exploring spatiotemporal changes of the urban heat Island effect in high-latitude cities at a neighbourhood level: A case of Edmonton, Canada. *Sustain. Cities Soc.* **2023**, *90*, 104403. [CrossRef]

26. Rizwan, A.M.; Dennis, L.Y.C.; Liu, C. A review on the generation, determination and mitigation of Urban Heat Island. *J. Environ. Sci.* **2008**, *20*, 120–128. [CrossRef] [PubMed]
27. Zhou, S.; Liu, D.; Zhu, M.; Tang, W.; Chi, Q.; Ye, S.; Xu, S.; Cui, Y. Temporal and Spatial Variation of Land Surface Temperature and Its Driving Factors in Zhengzhou City in China from 2005 to 2020. *Remote Sens.* **2022**, *14*, 4281. [CrossRef]
28. Hung, T.; Uchihama, D.; Ochi, S.; Yasuoka, Y. Assessment with satellite data of the urban heat island effects in Asian mega cities. *Int. J. Appl. Earth Obs. Geoinf.* **2006**, *8*, 34–48. [CrossRef]
29. Shahfahad; Bindajam, A.A.; Naikoo, M.W.; Horo, J.P.; Mallick, J.; Rihan, M.; Malcoti, M.D.; Talukdar, S.; Rahman, R.; Rahman, A. Response of soil moisture and vegetation conditions in seasonal variation of land surface temperature and surface urban heat island intensity in sub-tropical semi-arid cities. *Theor. Appl. Climatol.* **2023**, *153*, 367–395. [CrossRef]
30. Enete, A.A.; Madu, I.A.; Onwubuya, E.A. Climate change and the profitability of indigenous adaptation practices in smallholder agriculture in South East Nigeria. *Outlook Agric.* **2012**, *41*, 179–185. [CrossRef]
31. Zhang, C.; Xie, G.; Lu, C.; Liu, C.; Li, N.; Wang, S.; Sun, Y. The mitigating effects of different urban green lands on the heat island effect in Beijing. *Resour. Sci.* **2015**, *37*, 1156–1165. (In Chinese)
32. Liu, Y.; Yuan, Z.; Kong, W.; Sun, B.; An, B. The Changing Trend of Heat Island Intensity and Main Influencing Factors during 1993–2012 in Xian City. *J. Nat. Resour.* **2015**, *30*, 974–985. (In Chinese) [CrossRef]
33. Xiong, Y.; Zhang, F. Thermal environment effects of urban human settlements and influencing factors based on multi-source data: A case study of Changsha city. *Acta Geogr. Sin.* **2020**, *75*, 2443–2458. (In Chinese) [CrossRef]
34. Zhao, C.H.; Jensen, J.; Weng, Q.H.; Weaver, R. A Geographically Weighted Regression Analysis of the Underlying Factors Related to the Surface Urban Heat Island Phenomenon. *Remote Sens.* **2018**, *10*, 1428. [CrossRef]
35. Brunsdon, C.; Fotheringham, A.S.; Charlton, M. Some notes on parametric significance tests for geographically weighted regression. *J. Reg. Sci.* **1999**, *39*, 497–524. [CrossRef]
36. Wang, J.; Qian, Y.-G.; Han, L.-J.; Zhou, W.-Q. Relationship between land surface temperature and land cover types based on GWR model: A case of Beijing-Tianjin-Tangshan urban agglomeration, China. *Yingyong Shengtai Xuebao* **2016**, *27*, 2128–2136. (In Chinese) [CrossRef] [PubMed]
37. Kashki, A.; Karami, M.; Zandi, R.; Roki, Z. Evaluation of the effect of geographical parameters on the formation of the land surface temperature by applying OLS and GWR, A case study Shiraz City, Iran. *Urban Clim.* **2021**, *37*, 100832. [CrossRef]
38. Li, L.; Zha, Y.; Zhang, J. Spatially non-stationary effect of underlying driving factors on surface urban heat islands in global major cities. *Int. J. Appl. Earth Obs. Geoinf.* **2020**, *90*, 102131. [CrossRef]
39. Yu, Z.; Li, X.; Tursun, H. Research on Environmental Sustainability Degree in Urumqi. *J. Arid. Land Resour. Environ.* **2002**, *16*, 15–21. (In Chinese) [CrossRef]
40. Alimjan, A.; Amanguli, S.; Hui, L.I.U.; Turangul, H. Population development trend of Urumqi in future. *J. Arid. Land Resour. Environ.* **2011**, *25*, 32–38. [CrossRef]
41. Xuegang, C.; Zhaoping, Y. Study on Simulating Spatial Distribution and Varying Patterns of Population in Urumqi Based on GIS. *J. Arid. Land Resour. Environ.* **2008**, *22*, 12–16. (In Chinese) [CrossRef]
42. Xu, H.Q. Retrieval of the reflectance and land surface temperature of the newly-launched Landsat 8 satellite. *Chin. J. Geophys.-Chin. Ed.* **2015**, *58*, 741–747. (In Chinese) [CrossRef]
43. Sobrino, J.A.; Jiménez-Muñoz, J.C.; Paolini, L. Land surface temperature retrieval from LANDSAT TM 5. *Remote Sens. Environ.* **2004**, *90*, 434–440. [CrossRef]
44. Dong, X.; Tian, J.; Zhang, R.H.; He, D.X.; Chen, Q.M. Study on the Relationship between Soil Emissivity Spectra and Content of Soil Elements. *Spectrosc. Spectr. Anal.* **2017**, *37*, 557–565. (In Chinese) [CrossRef]
45. Seto, K.C.; Kaufmann, R.K. Modeling the drivers of urban land use change in the Pearl River Delta, China: Integrating remote sensing with socioeconomic data. *Land Econ.* **2003**, *79*, 106–121. [CrossRef]
46. Hidalgo-García, D.; Arco-Díaz, J. Modeling the Surface Urban Heat Island (SUHI) to study of its relationship with variations in the thermal field and with the indices of land use in the metropolitan area of Granada (Spain). *Sustain. Cities Soc.* **2022**, *87*, 104166. [CrossRef]
47. Wilson, J.S.; Clay, M.; Martin, E.; Stuckey, D.; Vedder-Risch, K. Evaluating environmental influences of zoning in urban ecosystems with remote sensing. *Remote Sens. Environ.* **2003**, *86*, 303–321. [CrossRef]
48. Brunsdon, C.; Fotheringham, A.S.; Charlton, M.E. Geographically Weighted Regression: A Method for Exploring Spatial Nonstationarity. *Geogr. Anal.* **1996**, *28*, 281–298. [CrossRef]
49. Md Bohari, N.F.; Kruger, E.; John, J.; Tennant, M. Analysis of dental services distribution in Malaysia: A geographic information systems—Based approach. *Int. Dent. J.* **2019**, *69*, 223–229. [CrossRef] [PubMed]
50. Brunsdon, C.; Fotheringham, A.S.; Charlton, M. Geographically weighted summary statistics—A framework for localised exploratory data analysis. *Comput. Environ. Urban Syst.* **2002**, *26*, 501–524. [CrossRef]
51. Guo, L.; Ma, Z.H.; Zhang, L.J. Comparison of bandwidth selection in application of geographically weighted regression: A case study. *Can. J. For. Res.* **2008**, *38*, 2526–2534. [CrossRef]
52. Ünal, Y.S.; Sonuç, C.Y.; Incecik, S.; Topcu, H.S.; Diren-Üstün, D.H.; Temizöz, H.P. Investigating urban heat island intensity in Istanbul. *Theor. Appl. Climatol.* **2020**, *139*, 175–190. [CrossRef]
53. Bechtel, B.; Demuzere, M.; Mills, G.; Zhan, W.; Sismanidis, P.; Small, C.; Voogt, J. SUHI analysis using Local Climate Zones—A comparison of 50 cities. *Urban Clim.* **2019**, *28*, 100451. [CrossRef]

54. Shahfahad; Naikoo, M.W.; Towfiqul Islam, A.R.M.; Mallick, J.; Rahman, A. Land use/land cover change and its impact on surface urban heat island and urban thermal comfort in a metropolitan city. *Urban Clim.* **2022**, *41*, 101052. [CrossRef]
55. Lu, L.; Weng, Q.; Xiao, D.; Guo, H.; Li, Q.; Hui, W. Spatiotemporal Variation of Surface Urban Heat Islands in Relation to Land Cover Composition and Configuration: A Multi-Scale Case Study of Xi'an, China. *Remote Sens.* **2020**, *12*, 2713. [CrossRef]
56. Amindin, A.; Pouyan, S.; Pourghasemi, H.R.; Yousefi, S.; Tiefenbacher, J.P. Spatial and temporal analysis of urban heat island using Landsat satellite images. *Environ. Sci. Pollut. Res.* **2021**, *28*, 41439–41450. [CrossRef]
57. Kaur, R.; Pandey, P. Spatial trends of surface urban heat island in Bathinda: A semiarid city of northwestern India. *Int. J. Environ. Sci. Technol.* **2022**, *19*, 10911–10932. [CrossRef]
58. Song, J.; Du, S.; Feng, X.; Guo, L. The relationships between landscape compositions and land surface temperature: Quantifying their resolution sensitivity with spatial regression models. *Landsc. Urban Plan.* **2014**, *123*, 145–157. [CrossRef]
59. Ma, X.L.; Peng, S.Y. Research on the spatiotemporal coupling relationships between land use/land cover compositions or patterns and the surface urban heat island effect. *Environ. Sci. Pollut. Res.* **2022**, *29*, 39723–39742. [CrossRef]
60. Cai, Y.B.; Zhang, H.; Zheng, P.; Pan, W.B. Quantifying the Impact of Land use/Land Cover Changes on the Urban Heat Island: A Case Study of the Natural Wetlands Distribution Area of Fuzhou City, China. *Wetlands* **2016**, *36*, 285–298. [CrossRef]
61. Saha, S.; Saha, A.; Das, M.; Saha, A.; Sarkar, R.; Das, A. Analyzing spatial relationship between land use/land cover (LULC) and land surface temperature (LST) of three urban agglomerations (UAs) of Eastern India. *Remote Sens. Appl. Soc. Environ.* **2021**, *22*, 100507. [CrossRef]
62. Njoku, E.A.; Tenenbaum, D.E. Quantitative assessment of the relationship between land use/land cover (LULC), topographic elevation and land surface temperature (LST) in Ilorin, Nigeria. *Remote Sens. Appl. Soc. Environ.* **2022**, *27*, 100780. [CrossRef]
63. Moisa, M.B.; Gemeda, D.O. Assessment of urban thermal field variance index and thermal comfort level of Addis Ababa metropolitan city, Ethiopia. *Heliyon* **2022**, *8*, e10185. [CrossRef]
64. Weng, Q.H.; Lu, D.S.; Schubring, J. Estimation of land surface temperature-vegetation abundance relationship for urban heat island studies. *Remote Sens. Environ.* **2004**, *89*, 467–483. [CrossRef]
65. Gao, Y.; Zhao, J.; Han, L. Exploring the spatial heterogeneity of urban heat island effect and its relationship to block morphology with the geographically weighted regression model. *Sustain. Cities Soc.* **2022**, *76*, 103431. [CrossRef]
66. Anniballe, R.; Bonafoni, S.; Pichierri, M. Spatial and temporal trends of the surface and air heat island over Milan using MODIS data. *Remote Sens. Environ.* **2014**, *150*, 163–171. [CrossRef]
67. Derdouri, A.; Murayama, Y.; Morimoto, T. Spatiotemporal Thermal Variations in Moroccan Cities: A Comparative Analysis. *Sensors* **2023**, *23*, 6229. [CrossRef] [PubMed]
68. Shahfahad; Talukdar, S.; Rihan, M.; Hang, H.T.; Bhaskaran, S.; Rahman, A. Modelling urban heat island (UHI) and thermal field variation and their relationship with land use indices over Delhi and Mumbai metro cities. *Environ. Dev. Sustain.* **2022**, *24*, 3762–3790. [CrossRef]
69. Chen, F.; Yang, S.; Yin, K.; Chan, P. Challenges to quantitative applications of Landsat observations for the urban thermal environment. *J. Environ. Sci.* **2017**, *59*, 80–88. [CrossRef]

Disclaimer/Publisher's Note: The statements, opinions and data contained in all publications are solely those of the individual author(s) and contributor(s) and not of MDPI and/or the editor(s). MDPI and/or the editor(s) disclaim responsibility for any injury to people or property resulting from any ideas, methods, instructions or products referred to in the content.